Geophysical Journal International

Geophys. J. Int. (2019) **217,** 894–905
Advance Access publication 2019 January 31
GJI Marine geosciences and applied geophysics

doi: 10.1093/gji/ggz068

Complex envelope retrieval for surface nuclear magnetic resonance data using spectral analysis

Lichao Liu,[1] Denys Grombacher,[1] Esben Auken[1] and Jakob Juul Larsen[2]

[1]*Department of Geoscience, Aarhus University, C. F. Møllers Alle* 4, 8000 *Aarhus C, Denmark. E-mail: lichao@geo.au.dk*
[2]*Department of Engineering, Aarhus University, Finlandsgade* 22, 8200 *Aarhus N, Denmark*

Accepted 2019 January 30. Received 2019 January 28; in original form 2018 August 27

SUMMARY

Aquifer properties can be obtained from envelopes of surface nuclear magnetic resonance (NMR) signals, but this demands high-quality data. To retrieve reliable envelopes using synchronous detection from the intrinsically low signal-to-noise ratio (SNR) surface NMR recordings, a variety of signal processing techniques are employed to mitigate noise. We present a different approach to retrieve complex envelopes using spectral analysis and a sliding window, which can potentially improve SNR significantly. The complex envelope is composed of the spectral values at the Larmor frequency found through the Fourier transform of surface NMR data using a sliding window. We discuss how to maximize the SNR of envelope by selecting the optimum length and shape of the sliding window. An accompanying method for determining the Larmor frequency is presented and we address how noise can deteriorate the envelope retrieval in spectral analysis. Results obtained from synthetic models and field measurements in low and high noise environments reveal that the proposed method not only improves the accuracy and efficiency of envelope retrieval, but also eliminates the transient distortion of early-time signal caused by the filtering procedure.

Key words: Hydrogeophysics; Time-series analysis; Instrumental noise.

1 INTRODUCTION

Surface nuclear magnetic resonance (NMR) is an emerging geophysical method capable of imaging subsurface aquifers (Legchenko & Valla 2002; Behroozmand *et al.* 2015). The NMR signal emitted by the stimulated hydrogen in groundwater is an exponentially decaying magnetic field oscillating at the Larmor frequency and it is recorded by the NMR instrumentation on the surface (Hertrich 2008). The NMR signal is characterized by its envelope, which is typically parametrized by an initial amplitude, relaxation time and relative phase between transmit pulse and received signal (Legchenko *et al.* 2002). The NMR signal amplitude directly indicates water content, the relaxation times are correlated with pore size and permeability (Lachassagne *et al.* 2005; Lubczynski & Roy 2005), and the phase arises from subsurface conductivity or off-resonance excitation (Trushkin *et al.* 1995; Grombacher *et al.* 2016). The full envelope or the parametrized envelope from the data is required for surface NMR inversions and groundwater interpretations (Legchenko & Shushakov 1998; Müller-Petke & Yaramanci 2010; Behroozmand *et al.* 2012). Therefore, accurate and reliable retrieval of the envelope is of critical importance for surface NMR investigations.

Field measurements are normally dominated by electromagnetic noise, especially in the proximity of anthropogenic infrastructure (Larsen & Behroozmand 2016). The most common noise sources include powerline harmonics, spikes typically originating from electric fences or thunderstorms and wide-band random noise (Dalgaard *et al.* 2012). The state-of-the-art strategy for envelope retrieval is synchronous detection in which the NMR signal is frequency-shifted to baseband through multiplication with a reference signal and subsequently low-pass filtered (Legchenko & Valla 2002; Müller-Petke *et al.* 2016). The steps of a modern surface NMR signal processing work flow are (Müller-Petke *et al.* 2016): (1) despiking (Dalgaard *et al.* 2012; Costabel & Müller-Petke 2014), (2) model-based harmonic subtraction (Larsen *et al.* 2014), (3) remote reference noise cancellation (Walsh 2008; Dalgaard *et al.* 2012), (4) stacking (Jiang *et al.* 2011) and (5) synchronous detection. Note that the synchronous detection step involves choosing a low-pass filter. Selecting the cut-off frequency for this filter involves compromising between the bandwidth of noise in the processed signal and duration of the filter transient (which corrupts the data at early times). Small cut-offs reduce noise levels but have long transients, while large cut-offs preserve more early time data but increase noise levels. The low-pass filters typically employed by users have a cut-off frequency of hundreds of Hz (Müller-Petke *et al.* 2016).

Irons & Li (2014) proposed a frequency domain approach for modelling and inversion of surface NMR data. This scheme differs from traditional synchronous detection approaches in that it does not extract the envelope, instead the initial amplitude and relaxation time are obtained through regressions within a frequency window around the Larmor frequency. However, only a few spectral bins with high magnitude around the Larmor frequency can be utilized in practice. This limitation becomes more severe when the relaxation time is long and the spectrum is correspondingly narrow.

We present an alternative method for retrieving NMR signal envelopes using spectral analysis. By exploiting the fact that the spectral magnitude at the Larmor frequency is proportional to the product of the initial amplitude and relaxation time, a high-SNR complex envelope can be extracted by Fourier transforming the data with a temporally sliding window, where the SNR is related to the length and shape of the window function. We discuss how to select these parameters to maximize SNR. In order to compute the envelope of the NMR signal accurately, the signal frequency applied in the Fourier transform must equal the Larmor frequency. We show how the Larmor frequency can be estimated by computing the Fourier transform for a range of frequency values and selecting the frequency, which produces the maximum spectral magnitude.

The major benefit of extracting the NMR signal envelope using spectral analysis is that only the noise at the frequency coincident with the Larmor frequency and spectrum leaked from other frequencies noise affect the extracted envelope. Hence the envelope SNR can potentially be improved significantly. Another important advantage is that spectral analysis avoids the filtering procedures in synchronous detection which eliminates the dead time associated with transient distortion from filters allowing envelopes to be extracted even from fast decaying signals. Spectral analysis is computationally efficient and real-time envelope extraction is easily implemented, aiding data quality control during field acquisition. A final benefit is that the spectral analysis approach produces data in the time-domain, which allows one to exploit existing familiarities with time-domain NMR data.

This paper is organized as follows. First, the principle of extracting envelopes using spectral analysis is introduced. Second, the algorithm implementation is described, as well as techniques for selecting the window length and shape, determining the Larmor frequency, and removing noise. Third, the effectiveness of spectral analysis is demonstrated with synthetic models and the ability to reproduce known envelopes is compared with standard envelope detection methods. Finally, two examples of the method applied to field data are presented.

2 METHOD

Surface NMR exploits the spin of protons in groundwater to generate signals. During a surface NMR measurement, an alternating current is injected into a transmit coil for a duration of tens of milliseconds. Once the pulse is terminated, the protons relax back to thermal equilibrium while emitting a weak magnetic field that oscillates at the Larmor frequency f_L. This signal, called a free induction decay (FID), is recorded with a receiver coil at the surface (Legchenko *et al.* 2002). Considering a single layered earth model the FID signal is given by

$$s(t) = s_0 e^{-t/T_2^*} \cos(2\pi f_L t + \varphi), \tag{1}$$

where the initial amplitude s_0 is proportional to the water content in the investigated volume, the effective transverse relaxation time T_2^* is determined by the pore size and the relative phase φ is related to the survey geometry, subsurface conductivity and excitation pulse parameters.

The Fourier transform of the NMR signal in eq. (1) can be written in the form of absorption and dispersion components (see the Appendix),

$$S(f) = e^{i\varphi}(S_a(f) + i S_d(f)), \tag{2}$$

where

$$\begin{aligned} S_a(f) &= \frac{s_0/T_2^*}{(1/T_2^*)^2 + 4\pi^2(f_L - f)^2}, \\ S_d(f) &= \frac{s_0 2\pi(f_L - f)}{(1/T_2^*)^2 + 4\pi^2(f_L - f)^2}. \end{aligned} \tag{3}$$

The width of the spectral line of the NMR signal is $1/(\pi T_2^*)$ Hz—the faster the decay, the broader the peak. At the Larmor frequency, the absorption spectrum reaches its maximum value while the dispersion component equals to zero and eq. (3) becomes

$$S(f_L) = s_0 T_2^* e^{i\varphi}. \tag{4}$$

The amplitude of the spectrum at the Larmor frequency is proportional to s_0 and T_2^* and the angle of the complex spectrum value remains consistent with the NMR phase. By repeatedly Fourier transforming the NMR signal using a sliding unit step function window $w(t) = u(t - t_s)$, which starts at t_s and extends to infinity, a time-series of complex spectral values at f_L can be obtained (Dabek *et al.* 2010).

The spectrum, $S_w(f, t_s)$ of the signal $s(t)$ windowed by a step function $u(t - t_s)$ is

$$S_w(f, t_s) = \mathcal{F}\{s(t_s : \infty)\}. \tag{5}$$

The time-series of spectral values at f_L, denoted as the scaled envelope $L(t_s)$, is

$$L(t_s) = S_w(f_L, t_s) = s_0 T_2^* e^{i\varphi} e^{-t_s/T_2^*} \tag{6}$$

with real and imaginary parts

$$\begin{aligned} \mathcal{R}\{L(t_s)\} &= s_0 T_2^* \cos(\varphi) e^{-t_s/T_2^*}, \\ \mathcal{I}\{L(t_s)\} &= s_0 T_2^* \sin(\varphi) e^{-t_s/T_2^*}. \end{aligned} \tag{7}$$

$L(t_s)$ is an exponentially decaying time-series with the same relaxation time as the NMR signal and it is the scaled envelope obtained with the proposed method. A schematic diagram of the NMR envelope extraction using spectral analysis with a sliding window is depicted in Fig. 1. After the excitation pulse is terminated, the usable NMR signal starts at t_{s0} with an initial amplitude of s_0. The fist complex value $L(t_{s0})$ is obtained by Fourier transforming the NMR signal windowed by the step function $u(t - t_{s0})$. The values $L(t_{s1})$ and $L(t_{s2})$ are computed after being windowed by step functions $u(t - t_{s1})$ and $u(t - t_{s2})$ respectively.

Since $t_s = 0$ corresponds to the start of the usable recording after the excitation pulse is terminated, the phase-corrected envelope after subtracting the phase of the excitation pulse is written as

$$L_c(t_s) = L(t_s) \cdot e^{-i\varphi_{corr}}, \tag{8}$$

where φ_{corr} is the phase related to the transmitting frequency and interval between the initial value of t_s and start time of excitation pulse.

3 ALGORITHM IMPLEMENTATION

For surface NMR measurements, the Larmor frequency ranges from about 1 to 3 kHz around the world. The oscillating NMR signal superimposed by noise is sampled with a frequency $f_s = 1/\Delta t$ between 19.2 and 50 kHz by state-of-the-art instruments (Walsh 2008; Radic & Lehmann-Horn ; Liu *et al.* 2019).

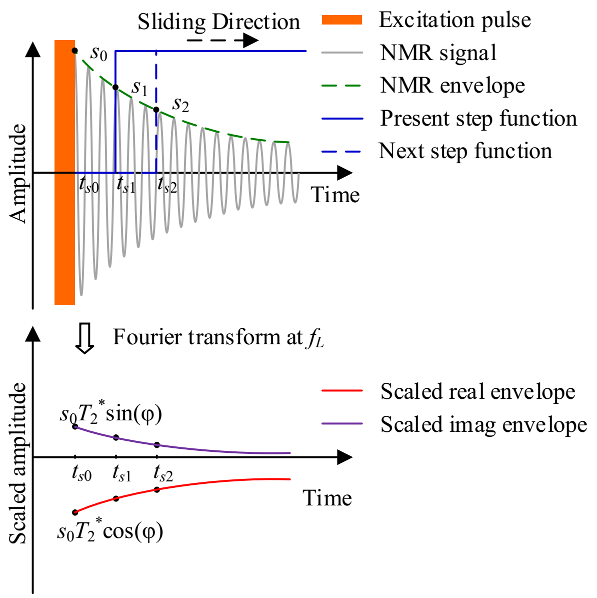

Figure 1. Schematic diagram of NMR envelope extraction using spectral analysis. A decaying NMR signal (black) starts from an initial amplitude s_0 and decays to s_1, s_2. The scaled real (red) and imaginary (purple) NMR envelope is obtained by Fourier transforming the data after multiplication by a sliding step function window (blue) plotted as starting at time t_{s1} (solid) and at time t_{s2} (dashed).

Using discrete time, the start of the window is written as $t_s = \mu k\Delta t$, $k \in \mathcal{N}$ where the constant μ controls the step length of t_s. If the retrieved envelope has a length of l_e, then the number of sliding windows is $\frac{l_e}{\mu\Delta t} + 1$. For a 32 μs sampling interval (as used in the Apsu instrument; Liu *et al.* 2019) μ values used are around 10–500 according to the expected relaxation times of the NMR signal: Fast decaying signals (T_2^* is roughly less than 150 ms) require small μ to have dense data points in the early time, while longer relaxation time signals require larger μ to reduce the number of data points in the envelopes which can improve the efficiency of the inversion algorithms. The step length has the same functionality as the resampling techniques described by Müller-Petke *et al.* (2016).

In the implementation of the proposed approach, only a finite number of samples can be used in the Fourier transform as the length of a record is limited by the interval between two adjacent excitation pulses and because the signal disappears into noise at the later part of the record. The truncation of the observed signal corresponds to multiplication with a rectangular window. Therefore, the window function becomes $w(t) = u(t - t_s) - u(t - (t_s + l_w))$, where l_w is the window length which can be expressed in number of samples N: $l_w = N\Delta t$. The value of a windowed NMR signal is written as,

$$S_w(f_L, t_s) = \Delta t \sum_{k=0}^{N-1} s(k\Delta t)w(k\Delta t)e^{-i2\pi f_L k\Delta t}. \tag{9}$$

Effectively, this is a discrete time Fourier transform (DFT) at the Larmor frequency. The Fourier transform can also be interpreted as an N-order bandpass finite impulse response (FIR) filter given by the convolution between the frequency response of the window function w and the Dirac delta function $\delta(f - f_L)$ (Smith 2011). Therefore, the frequency response of the window function can be used to evaluate the performance of DFT. The main difference between the DFT and the standard bandpass filter is that the former has no transient distortion as future-directed data are used rather than past-directed data.

3.1 Window length

The window function is characterized by its length and shape, both of which have impacts on the SNR of the retrieved envelope in the proposed method. Initially, we focus on a rectangular window. First, a short window cannot encompass all of the NMR signal in the scenario of a long relaxation time. The values of T_1, T_2 and T_2^* of water-saturated material relevant for geological application range from a few ms for samples containing magnetic material to more than 1 s for clean quartz sands (Keating & Knight 2006). Field measurements in different locations in Denmark typically give T_2^* values less than 0.4 s (Vilhelmsen *et al.* 2014). The spectral value at f_L of a rectangle windowed NMR signal is given by

$$S_w(f_L; t_s) = s_0 T_2^* e^{i\varphi} e^{-t_s/T_2^*}(1 - e^{-l_w/T_2^*}). \tag{10}$$

The consequence of using a short window is that the complex envelope gets multiplied by the factor $1 - e^{-l_w/T_2^*}$, which depends on T_2^* and l_w. This leads to under-estimated signal amplitudes, for example, 63.2 , 86.5, 95.0 and 98.2 per cent of $s_0 T_2^*$ for l_w values of 1, 2, 3 and 4 times T_2^*, respectively. If l_w is approximately four times the signal relaxation time or more, the truncation effect of the window length can be ignored and there is no need to correct for it.

Second, the window length should be sufficiently long as it determines the frequency resolution $\Delta f = 1/l_w$ in spectral analysis. From the viewpoint of a filter, the width of the passband of the DFT is Δf. The frequency response of an N-sample rectangle window function is

$$H(e^{i\omega}) = \frac{e^{-i\omega N/2}}{e^{-i\omega/2}} \frac{\sin(\omega N/2)}{\sin(\omega/2)}, \tag{11}$$

where $\omega \in [-\pi, \pi]$ is the normalized angular frequency. The equivalent noise bandwidth n_{bw} of an l_w long rectangle window is $1/l_w$, for instance a window length of 1 s results in a 1 Hz noise bandwidth. Therefore, a longer window has narrowed noise bandwidth and hence more noise attenuation. Compared to a low-pass filter with bandwidth B_w applied in the traditional approach, the proposed method can potentially reduce the noise RMS value by a factor of $\sqrt{B_w/n_{bw}}$.

However, an NMR signal decays whereas dominant noise sources such as instrument noise and powerline harmonics are stationary or near-stationary throughout a measurement. The average spectral magnitude of an NMR signal decreases when l_w increases due to the decay. Thus a longer window may result in a decreased SNR, especially when the relaxation time of the NMR signal is short. The noise with RMS value δ_n can be written in the form of noise spectral density $\nu(f)$, assumed to be band-limited to the frequency range $f_1 < f < f_2$,

$$\delta_n = \sqrt{\int_{f_1}^{f_2} \nu^2(f)df}. \tag{12}$$

The SNR of the retrieved envelope is defined as the spectral magnitude ratio between the scaled envelope and the noise at the Larmor frequency (Spencer 2010),

$$\mathrm{SNR}(f_L) = \frac{s_0 T_2^*(1 - e^{-l_w/T_2^*})}{\nu(f_L)\sqrt{l_w}}. \tag{13}$$

The noise at the Larmor frequency consists of the noise within the signal frequency f_L bin (referred to as co-frequency) and the components, for example, powerline harmonics, leaked into f_L from other frequencies, due to the side lobes of the window function. It can be mathematically demonstrated that SNR(f_L) is maximized when l_w equals 1.25 T_2^* for NMR signals superimposed by Gaussian noise.

In conclusion, the length of rectangular window should be long enough to encompass the majority of the NMR signal and the optimum l_w depends on T_2^* and the noise environment. In practice, where an unknown T_2^* is to be determined, a 0.5 s long window can be employed in an initial processing. At the end of a 0.5 s window, a signal with $T_2^* = 0.2$ s decays to only 8.2 per cent of its initial value and the window covers the majority of the signal information.

3.2 Window shape

To further improve SNR in the spectral analysis method, a shaped window function can be used to impose preferential weighting on the initial high-SNR part and less on the late time data dominated by noise. A convenient choice of shaped window function is the exponential window

$$w(t) = \mathrm{e}^{-t/T_w}, \tag{14}$$

where T_w is the decay rate of the weighting function. The weighted and transformed NMR signal is given by

$$L(t_s) = s_0 T_c \mathrm{e}^{-t_s/T_2^*}(1 - \mathrm{e}^{-l_w/T_c}), \tag{15}$$

with the comprehensive time constant

$$T_c = \frac{T_2^* T_w}{T_2^* + T_w}. \tag{16}$$

After applying the window function, both the NMR signal and the noise are suppressed. From eq. (16) it is seen that T_c is smaller than T_2^*, which implies that the spectral peak becomes smaller and wider. Importantly, the retrieved envelope L preserves the relaxation rate T_2^* because all the spectral values obtained with the temporally sliding window are scaled with the same factor $\frac{T_c}{T_2^*}\frac{1-\mathrm{e}^{-l_w/T_c}}{1-\mathrm{e}^{-l_w/T_2^*}}$.

A faster decaying weighting function will remove more noise but the spectral magnitude of the NMR signal will also become smaller. The SNR of the spectrum after applying the exponential weighting function is (Spencer 2010)

$$\mathrm{SNR}_w(f_L) = \frac{s_0 T_c (1 - \mathrm{e}^{-l_w/T_c})}{\nu\sqrt{\frac{T_w}{2}(1 - \mathrm{e}^{-2l_w/T_w})}}. \tag{17}$$

The SNR is maximized when the decay rate of the exponential weighting function matches the relaxation rate of the NMR signal. A numerical study of this is depicted in Fig. 2. Synthetic models with different relaxation times from 0.1 s to 0.5 s are superimposed by the Gaussian random noise and different window functions are used to retrieve the NMR signal. The RMS of the random noise is 10 times of the initial amplitude of NMR signal. The sampling frequency is 31.25 kHz and windows with a length of 1 s are used.

The SNR is low when the decay rate is fast and increases significantly as T_w goes up. The SNR reaches its peak value when T_w equals T_2^* and decreases slowly as T_w is further increased. When T_w exceeds T_2^*, the SNR of signals with long relaxation times decrease slower than that with short relaxation times. In cases where T_2^* is unknown, we recommend choosing a preliminary decay rate of 0.25 s as it will ensure high SNR in most scenarios. Once a T_2^* value is estimated, it can be used in a second iteration as the decay rate of the window function to increase SNR.

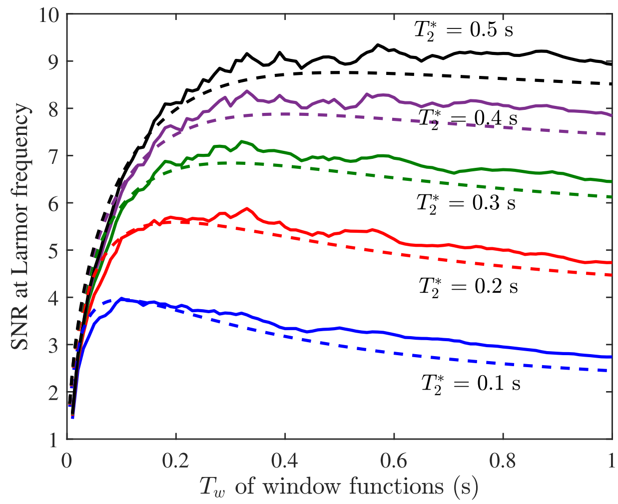

Figure 2. SNR of an NMR spectrum obtained by Fourier transforming signals with relaxation times of 0.1 s (blue), 0.2 s (red), 0.3 s (green), 0.4 s (purple) and 0.5 s (black) multiplied by different exponentially decaying window functions. The solid lines are simulation results and the dashed lines are theoretical values computed with eq. (17).

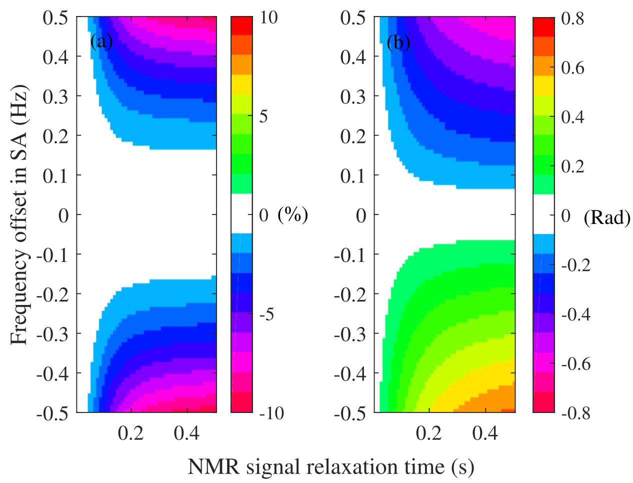

Figure 3. Relative errors of estimated (a) amplitude and (b) phase using spectral analysis on signals with different relaxation times (*x*-axis) and different frequency offsets (*y*-axis).

3.3 Larmor frequency determination

The proposed method requires an input Larmor frequency $\hat{f}_L$ for the Fourier transform, but in practice the accurate value of f_L is unknown because of measurement uncertainty in magnetometer readings, limits on spectral resolution because of the short signal duration, temporal variations of the Earth's magnetic field and/or magnetic anomalies in the subsurface. An offset Δf_L between the true Larmor frequency and the assumed frequency $\hat{f}_L$ can result in an underdetermined amplitude and inaccurate phase information when using spectral analysis, similar to how a frequency offset also causes problems with synchronous detection. Results from a simulation of this problem, conducted to evaluate the amplitude and phase errors caused by Δf_L, are presented in Fig. 3. The window utilized in the calculation is a 0.5 s square window.

When Δf_L is less than 0.25 Hz, the relative amplitude error is less than 2.5 per cent. For Δf_L less than 0.17 Hz, the relative amplitude error is smaller than 1 per cent (the white area). For relaxation times

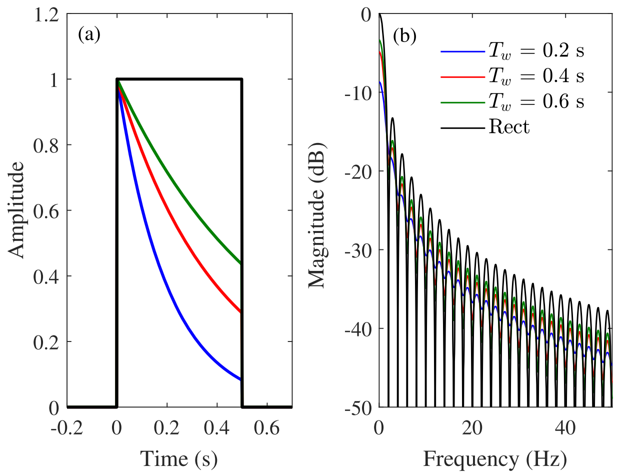

Figure 4. (a) Time domain waveforms and (b) frequency responses of 0.5-s-long window functions including rectangle (black), exponential with decay rates $T_{\rm w} = 0.2$ s (blue), 0.4 s (red) and 0.6 s (green) windows.

$T_2^* > 0.2$ s and a $\Delta f_{\rm L}$ of approximately 0.5 Hz, the relative amplitude error is increased but still less than 10 per cent. The phase error is more sensitive to a frequency offset, and it could reach 0.6 rad when $\Delta f_{\rm L}$ is close to 0.5 Hz. When $\Delta f_{\rm L}$ is less than 0.25 Hz and T_2^* is shorter than 0.3 s, the phase error is within 0.1 rad. As a rule of thumb, the frequency offset should be less than 0.25 Hz in the spectral analysis method.

A fast and simple approach to determine $f_{\rm L}$ accurately is to repeat the Fourier transform multiple times with different $\hat{f}_{\rm L}$ in a given range, for example, ±0.5 Hz from the Larmor frequency calculated from local Earth's field measurement. The optimum $\hat{f}_{\rm L}$ will yield the maximum spectral magnitude as demonstrated in Fig. 3(a). Stacking recorded time-series can improve the accuracy of $\hat{f}_{\rm L}$ estimates. The determination of Larmor frequency for one measurement will be conducted once. The recordings from the same pulse moments are averaged and the stacked data which has the highest SNR is used to evaluate the Larmor frequency. Afterwards, the determined Larmor frequency will be applied in the Fourier transform for all the pulse moments.

3.4 Noise considerations and uncertainty estimates

The DFT can be viewed as a narrow bandpass filter which is the convolution between the frequency response of the window function and the Dirac delta function $\delta(f - f_{\rm L})$. The waveform and frequency response of 0.5-s-long rectangular and exponentially decaying window functions are plotted in Fig. 4.

The exponential window has more attenuation in the main lobe compared to the rectangle window. Although the rectangle window has less attenuation at frequencies $(k - 0.5)\Delta f$, it can reduce the frequency components $k\Delta f$ to zero ($k = 1, 2, 3,$). A 38 dB (80 times) attenuation can be achieved when the difference between $f_{\rm L}$ and noise frequency is more than 50 Hz. When the window length increases, the attenuation is even higher. Recorded signals are normally severely distorted by noise in the time-series. The noise mainly consists of instrument noise, powerline harmonics, spikes and other electromagnetic noise. In the spectrum, noise inside the main lobe (co-frequency noise) and distributed in the side lobes of the frequency response of the window functions can leak into the NMR signal bin and distort the envelopes retrieved with the spectral analysis method.

Instrument noise is normally uniformly distributed, also in the frequency range close to the Larmor frequency. The noise spectral density of untuned surface NMR receivers is about 0.5 nV Hz$^{-1/2}$-1.8 nV Hz$^{-1/2}$ (Walsh 2008; Radic & Lehmann-Horn ; Liu *et al.* 2019). Instrument noise is incoherent and can only be reduced by stacking. An $N_{\rm s}$-fold stacking can reduce the random noise by a factor of $\sqrt{N_{\rm s}}$ at the expense of increased measurement time in the field. In most scenarios, instrument noise accounts for only a slight portion of the noise.

Power line harmonics have a comb-like spectrum and typically have higher magnitudes than other noise sources. With respect to spectral analysis, the power line harmonics are categorized into two types: the co-frequency component ($|f - f_{\rm L}| < \Delta f$) and non-co-frequency components. According to the frequency response in Fig. 4, the attenuation is more than 13 dB out of the passband. For frequency offsets exceeding 50 Hz, the attenuation is more than 38 dB. In most cases, the non-co-frequency power line harmonics are significantly attenuated by the combined action of stacking and the filtering done with the Fourier transform and it is not necessary to remove them with, for example, model-based methods.

For the co-frequency harmonic, coherent averaging will reduce this as the phase of NMR signal is fixed while the phase of harmonic vary in repeated measurements. If the stacked co-frequency harmonic still distort the NMR signal, it can be removed with a model-based methods (Larsen *et al.* 2014). In scenarios where the parameters of power line harmonics vary rapidly, the co-frequency harmonic can be removed using reference coil based methods (Liu *et al.* 2018). If necessary, remote reference noise cancellation can also be applied to remove noise including the co-frequency noise prior to spectral analysis (Larsen *et al.* 2014; Müller-Petke *et al.* 2016). Impulsive noise from, for example, thunderstorms or electrical fences is referred to as spikes and can have a much higher magnitude than the normal recording level. The transient character of this noise implies a similar wide spectrum and the noise will affect the NMR signal. Hence, spikes need to be removed before Fourier transforming. We use weighted stacking to remove spikes. A spike is identified if the amplitude exceeds a threshold defined by five times the median of the absolute value of the record and the spike-contaminated segment is applied a zero weight in stacking.

Stacking the time-series and subsequently using spectral analysis to extract envelopes on the stacked data can speed up the algorithms. Due to the linearity of the Fourier transform, the obtained envelopes are intrinsically the same as envelopes extracted using spectral analysis on the individual time-series and then stacking the envelopes. By stacking the time-series first, the number of DFT calculations is reduced by a factor equal to the number of stacks. The uncertainties of an envelope are computed from noise-only data, which are obtained by stacking an even number of records with alternating signs. Because the phase of the NMR signal is consistent from stack to stack, the NMR signal will be cancelled due to the alternating sign leaving only the noise in the stacked time-series. Then, the signal-cancelled data is processed using the same procedure as the signal-containing data to yield a noise-only envelope. The absolute values of this noisy envelope are treated as the corresponding uncertainty of the signal envelope. These uncertainties are based on the stacked noise data, hence they are smaller than the standard deviation computed during stacking of envelopes. In most scenarios, they are good estimates of the envelope uncertainty, because the phase of the noise varies from stack to stack. In the unlikely case where the noise phase is constant over adjacent stacks, the computed uncertainties becomes zero and cannot be used.

In summary, the work flow of the proposed method is:

(1) de-spiking,
(2) model-based co-frequency noise subtraction or reference noise cancellation if necessary,
(3) stacking,
(4) determine $\hat{f}_L$,
(5) DFT with sliding window,
(6) uncertainty estimation.

4 SIMULATION RESULTS

We demonstrate the performance of spectral analysis for the retrieval of envelopes and estimation of signal parameters in the following using synthetic signals embedded in noise-only recordings. Continuous noise-only data was recorded using the Apsu instrument in a 10×10 m^2, eight-turn Rx loop at a test-site near Aarhus, Denmark (Liu *et al.* 2019). The instrument has a bandpass filter with cut-off frequencies of 1 and 5 kHz to suppress low order power line harmonics and radio-frequency noise. Data are sampled at 31.25 kHz. The Rx loop was located in a farmland approximately 500 m away from an overhead high-voltage power line and a highway. Residential dwellings are located approximately 1 km away.

The synthetic signals have constant phase $\varphi = 1$ rad and frequency $f_L = 2150$ Hz, which is the typical Larmor frequency in Aarhus, Denmark. Twenty evenly spaced initial amplitude values between 10 and 200 nV, and 25 evenly spaced relaxation times between 0.02 and 0.5 s compose 500 synthetic signal models. We use a constant phase in the synthetic signals as the envelope SNR has been found to be mainly affected by initial amplitude and relaxation time. For each choice of signal parameters, 320 segments of 1 s are extracted with an interval of 5 s from the continuous noise-only recordings.

Before embedding the synthetic signal, the noise floor is evaluated as follows: Spikes and power line harmonics excluding the co-frequency harmonic are removed in each segment. The co-frequency harmonic is removed by three steps: (1) modelling the co-frequency on the data 1 s before the 'signal' segment, (2) extrapolating the modelled waveform to the 'signal' segment and (3) subtracting the extrapolated waveform from the 'signal' segment. After noise reduction, 32 segments are stacked to create a single noise-only data set, resulting in 10 noisy time-series in total. The RMS value δ_n of the 10 stacked noise-only time-series ranges from 114 to 217 nV. The noise after removal of power line harmonics and spikes mainly originates from random noise and hence $\nu(f)$ is estimated to be between 1.8 and 3.4 nV Hz$^{-1/2}$ according to the cut-off frequencies of the instrument. The spectral magnitudes of noise-only data around 2150 Hz (a) before and (b) after removing co-frequency harmonic are shown in Fig. 5. The magnitude at 2150 Hz ranges from 2 to 8 nV Hz$^{-1/2}$ and drops to 0.1 to 1.6 nV Hz$^{-1/2}$ after removal of co-frequency noise. The magnitudes at other frequencies range between 1 and 2.8 nV Hz$^{-1/2}$, which match the calculated noise spectrum density.

Finally, each of the 500 synthetic signals is each embedded in 10 of the original, unprocessed noise-only records. This produces a total of 5000 synthetic models, which are noise reduced as described above before we apply the spectral analysis method.

4.1 Larmor frequency

A 0.5-s-long rectangle window is applied in the determination of Larmor frequency and the frequency is swept from 2149.5 to 2150.5 Hz in 0.05 Hz increments. The estimated f_L is the one yielding the maximum amplitude. The range of estimated Larmor frequencies are shown in Fig. 6.

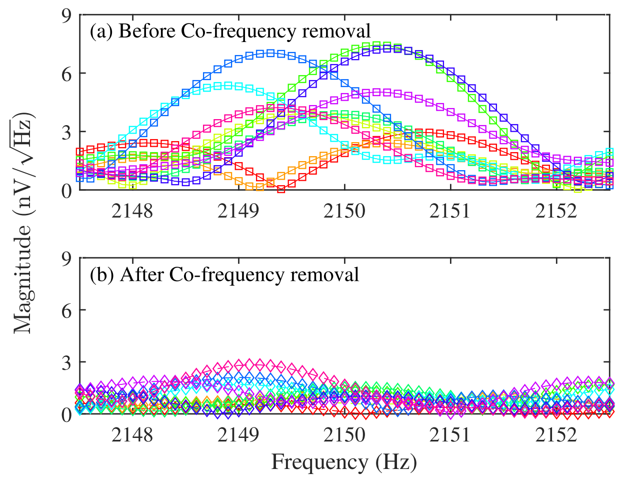

Figure 5. Spectral magnitudes of stacked noisy data around $f_L = 2150$ Hz (a) before and (b) after cofrequency harmonic removal. Different colours correspond to different noisy time-series.

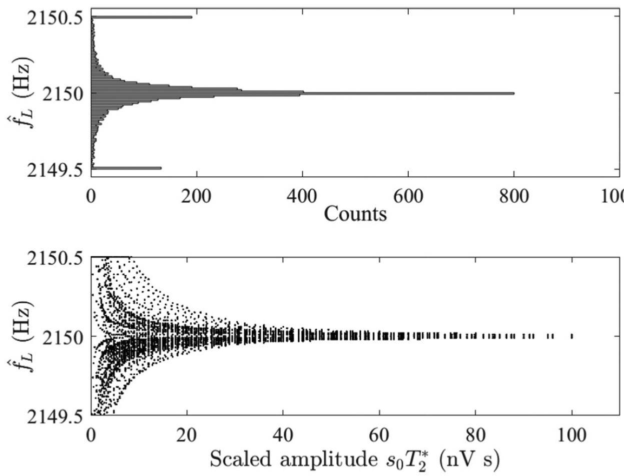

Figure 6. Statistics of the estimated Larmor frequency from synthetic signals with a frequency of $f_L = 2150$ Hz. (a) Histogram of 5000 estimates, and (b) scatter plot of estimated f_L (y-axis) versus scaled amplitude $s_0T_2^*$ (x-axis).

In Fig. 6(a), the estimated $\hat{f}_L$ is 2150.00 ± 0.16 Hz and 92 per cent of the estimates are within [2149.75, 2150.25] Hz. Due to the boundaries on the search frequencies, there are 190 and 132 estimates located at the edges of 2150.5 and 2149.5 Hz, respectively. These estimates are obtained when s_0 or T_2^* is small, which is demonstrated in Fig. 6(b). When the scaled amplitude is smaller than 5 nVs, the Larmor frequency is poorly determined resulting in some of the estimates being located at the search boundaries. When the scaled amplitude $s_0T_2^*$ is more than 15 nV s the estimates always lie within [2149.75, 2150.25] Hz and when $s_0T_2^*$ is more than 30 nV s, the f_L is well-determined and can be located within [2149.9, 2150.1] Hz. This is because the fluctuation in the spectral magnitudes within [2149.5, 2150.5] Hz is approximately 0.3 nV, while the relative error in magnitudes due to $\pm$ 0.5 Hz offsets between the true and estimated Larmor frequencies is about 10 per cent. When $s_0T_2^*$ is more than 30 nV s, the error magnitude due to frequency offset is more than the noise fluctuation. The detection threshold of scaled

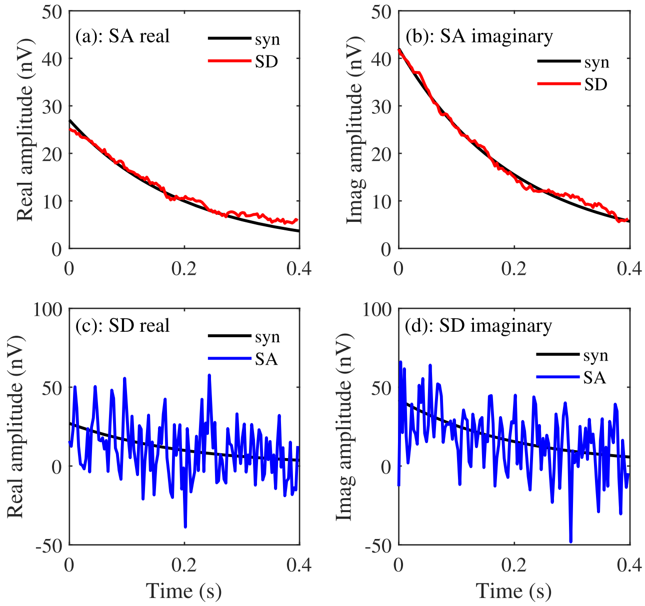

Figure 7. One example of the extracted (a) real and (b) imaginary envelopes using SA (red) and (c) real and (d) imaginary envelopes using SD (blue). The amplitude obtained in SA is calibrated by using eq. (10) after fitting the T_2^*. The real and imaginary envelopes (black) of synthetic signal with $s_0 =$ 50 nV, $T_2^* = 0.2$ s and $\varphi = 1$ rad.

amplitudes in these noise data is 15 nV s. The threshold $s_0 T_2^* =$ 15 nV corresponds to $s_0 = 75$ nV for $T_2^* = 200$ ms. The scaled amplitude threshold 15 nV s is noise dependent. When the noise is lower, the threshold becomes lower.

4.2 Envelope retrieval

In the following, the spectral analysis (SA) and synchronous detection (SD) approaches are used to extract envelopes from all 5000 synthetic models. The retrieved envelopes and estimated parameters are compared to evaluate the performance of the SA method. The signal frequency in SA and the reference signal in SD are both 2150 Hz. In SA, the step size μ is 100, the exponential window length l_w is 0.5 s, and the decay rate T_w is 0.25 s for all synthetic signals. In SD, a 1000 Hz wide bandpass filter with 60 dB attenuation is used to remove noise before applying the SD method. After the SD, a 500 Hz stopband, 60 dB attenuation low-pass filter is utilized to suppress noise further. The SD envelope is resampled with a interval of 3.2 ms.

Fig. 7 shows the retrieved real and imaginary envelopes from a synthetic signal ($s_0 = 50$ nV and $T_2^* = 0.2$ s) by SA and SD. The scaled amplitude of the synthetic signal is $s_0 T_2^* = 10$ nV and the noise density is 1.2 nV Hz$^{-1/2}$ in this data. The amplitude obtained in SA is calibrated using eq. (10) after fitting T_2^* for comparison. The envelopes retrieved by SA (red) have significant SNR improvements and fit the synthetic curve (black) accurately. The envelopes obtained by SD (blue) track the synthetic curve but have much more noise. The SD approach has a dead time of approximately 5 ms as determined from the distorted part of the of the extracted envelopes from a noise-free synthetic signal using the same filters. In contrast, the SA envelopes have no early-time distortion and track the synthetic curve from the beginning of the records. Results obtained with different signal parameters show similar behaviour: the SA

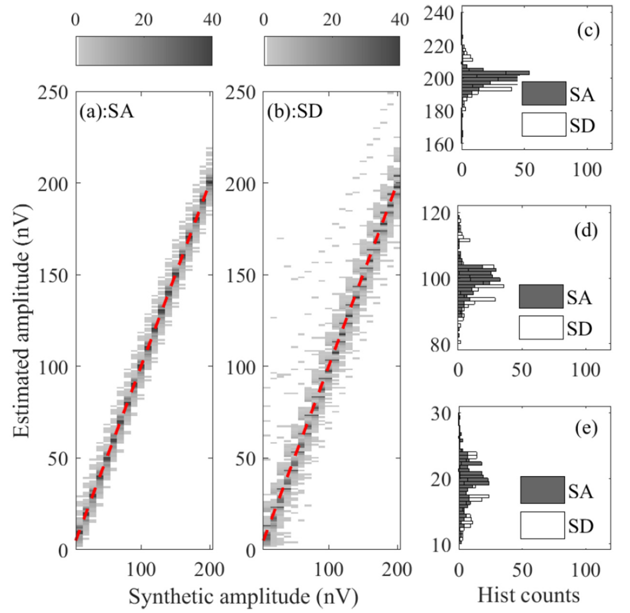

Figure 8. Comparison between the estimated initial amplitudes using (a) SA and (b) SD methods. The red dashed line in (a) and (b) is the 1:1 slope which indicates the true values. The estimates from the synthetic values s_0 = 200, 100 and 20 nV are shown in (c), (d) and (e), respectively.

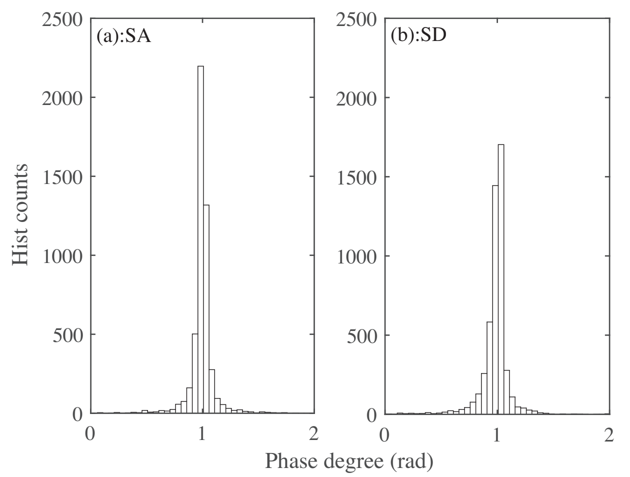

Figure 10. Histogram distributions of estimated phase using (a) SA and (b) SD methods, where the true phase is 1 rad.

results show characteristic NMR envelopes while the SD results are noisy and NMR envelopes are barely visible with the naked eye.

4.3 Parameter estimates

To evaluate the accuracy of the SA method in comparison with SD, mono-exponential decays are fitted to the processed data using nonlinear curve fitting (Legchenko & Valla 1998). To obtain comparable results, the amplitude obtained with SA is calibrated by eq. (10) after fitting T_2^*. Initial amplitudes, relaxation times and phase are shown in Figs 8–10, respectively.

In Fig. 8(a), initial amplitudes produced by SA have smaller deviations and higher estimate accuracy compared to the results obtained using the SD approach in Fig. 8(b). The SA estimates match the true

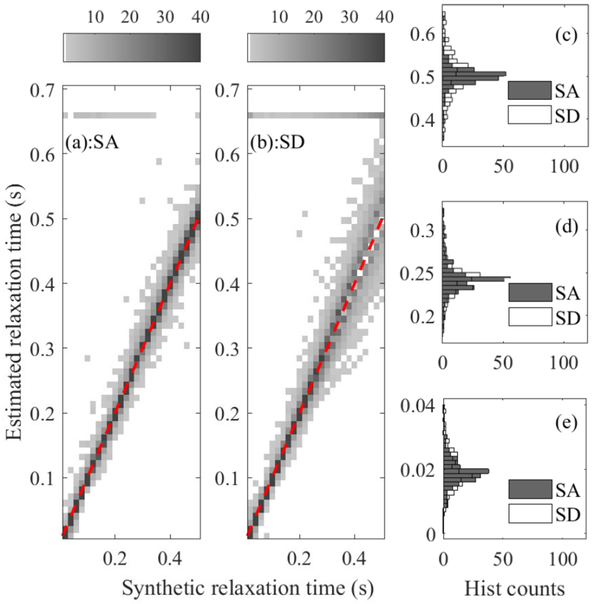

Figure 9. Comparison between the estimated relaxation times using (a) SA and (b) SD methods. The red dashed line in (a) and (b) is the 1:1 slope which indicates the true values. The estimates from the synthetic values $T_2^* = 0.5$, 0.25 and 0.02 s are shown in (c), (d) and (e), respectively.

value line precisely through all synthetic amplitudes. In Fig. 8(b), although the envelopes retrieved by SD are very noisy, the least-squares nonlinear regression algorithm can still yield useful results, but larger deviations and more outliers are seen in the SD approach, especially when the initial amplitudes are smaller than 50 nV. The results, plotted as histograms in Figs 8(c)–(e), show that both SA and SD produce good estimates when the initial amplitude is high, but the results obtained by SA match the true values better with smaller deviations and have fewer estimated values differing from the true values, which in turn implies that SA has higher accuracy for estimating initial amplitudes.

As seen in Figs 9(a) and (b) the SA produces small deviation and higher estimate accuracy for relaxation times compared to the SD approach, especially when the relaxation time is long. The increased deviation in the long relaxation times is caused by the small initial amplitude, but the distribution of SA is closer to the red dashed line when the relaxation times is around 0.5 s. Because the SA method is not strongly affected by the noise at other frequencies, it can produce accurate relaxation time estimates even when the signal amplitude is small. In Figs 9(c)–(e), the SA histograms are more narrowly distributed around the synthetic values than the SD histograms, which implies that SA has higher estimation accuracy.

Fig. 10 shows the estimated phase histograms by SA and SD. The SA results have more values at the synthetic phase 1 rad. The estimated phase is 0.99 ± 0.18 rad using SA and 0.97 ± 0.23 rad using SD, respectively. The mean value and standard deviation of the estimated phase are computed from the 5000 synthetic models. The true Larmor frequency is used both in the Fourier transform for SA and as the reference signal frequency in SD. Both methods yield good estimates of phase with SA giving a slightly more accurate value than SD.

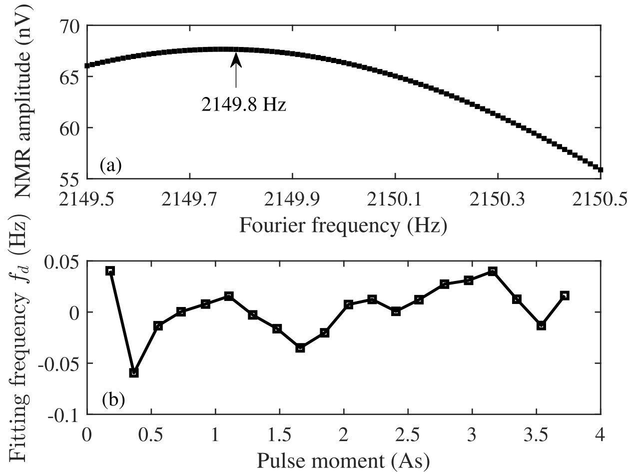

Figure 11. (a) Estimation of the Larmor frequency in the 2 As pulse moment data by sweeping the Fourier frequency between 2149.5 and 2150.5 Hz. (b) Deviations from the estimated Larmor frequency by nonlinear regression on the extracted envelope.

5 FIELD MEASUREMENTS

5.1 Low noise scenario

A groundwater investigation was conducted in Kompedal forest near Silkeborg, Denmark in May 2018. Prior NMR and TEM measurements at the site indicate a thick, resistive unit (interpreted to be a thick sand layer) extending to a depth of 30 m is underlain by a more conductive unit (interpreted to be a finer sand/clayey sand layer; Grombacher *et al.* 2018). The site is 1.5 km away from the closest village and has a low noise level. The local Larmor frequency was observed to be 2150 Hz. Surface NMR data were recorded using 40 ms on-resonance pulses with pulse moments ranging from 0.18 to 3.8 A s. Eight stacks were recorded for each pulse moment. The transmitter loop was a 50×50 m^2, single turn square coil. The receiver loop was a 9×9 m^2, 12-turn coil placed at the centre of the Tx loop (Behroozmand *et al.* 2016).

The raw data were stacked and processed with spectral analysis method. The RMS value of stacked data ranges from 90 to 120 nV and the noise spectral density is approximately 1.5 nV Hz$^{-1/2}$. The powerline harmonics had high amplitudes at low orders but were weak at frequencies higher than 1.8 kHz. The co-frequency harmonic noise of the noisy data measured by stacking the recordings with alternative polarity has a magnitude of approximately 2 nV. Except stacking, no more noise reduction techniques are used. Because the typical relaxation times of the signals range between 0.15 and 0.3 s, a 0.5 s rectangle window length is used. The co-frequency noise is weak and there is no need to apply the exponential window. The sliding step is 50 samples and the window is moved 320 times.

The Larmor frequency is observed to be 2150 Hz with a magnetometer. The true Larmor frequency is estimated using the method described in Section 3.4. The stacked time-series measured with a pulse moment of 2 As is used. The amplitudes computed by using different signal frequencies in the Fourier transform are shown in Fig. 11(a). The maximum spectral magnitude is obtained at 2149.8 Hz as indicated by the arrow. This frequency is used in the spectral analysis method to extract envelopes from all pulse moments. After envelope retrieval, the accuracy of the Larmor frequency estimation is verified by fitting the data to the envelope

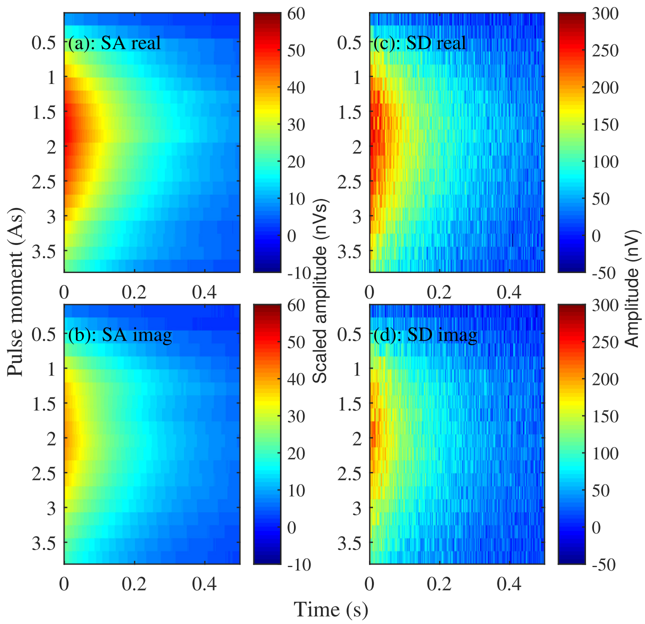

Figure 12. Retrieved (a) real and (b) imaginary envelopes of different pulse moments (y-axis) using spectral analysis from data collected at Kompedal forest, Denmark. (c) and (d) are the real and imaginary envelopes extracted using synchronous detection. The colour indicates the scaled amplitude $s_0 T_2^*$ in the SA method.

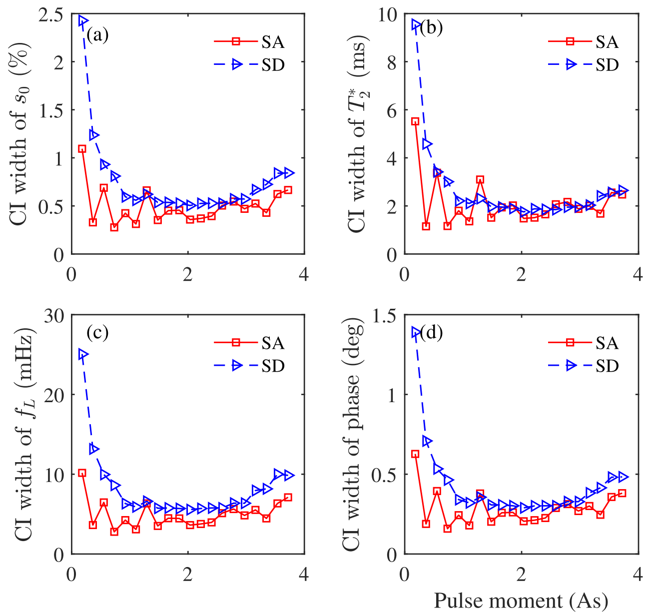

Figure 13. The confidence intervals of estimated parameters from extracted envelopes using spectral analysis (red square) and synchronous detection (blue triangles): (a) the CI of s_0 divided by the estimated s_0; (b–d) the CIs of estimated T_2^*, f_L and φ.

model,

$$\mathcal{R}\{L(t_s)\} = s_0 T_2^* \cos(2\pi f_d + \varphi) e^{-t_s/T_2^*},$$
$$\mathcal{I}\{L(t_s)\} = s_0 T_2^* \sin(2\pi f_d + \varphi) e^{-t_s/T_2^*}, \quad (18)$$

where f_d is the frequency difference between the true Larmor frequency and 2149.8 Hz. The results of fitting f_d are shown in Fig. 11(b). We find f_d values in the range −0.06 to 0.05 Hz. Hence, the estimated 2149.8 Hz is more accurate than the 2150 Hz observed by the magnetometer and we use this value for the Larmor frequency.

Synchronous detection is compared with the spectral analysis method. For SD, a 1 kHz bandpass filter is applied first and model-based subtraction is then used to remove the powerline harmonics excluding the 2150 Hz component. Subsequently, the envelopes are extracted using SD and a 500 Hz lowpass filter after stacking. The retrieved envelopes are shown in Fig. 12.

In the low noise environment, both SA and SD extract high quality envelopes. With SA, the SNR of the retrieved envelopes range from 10 to 50 in the spectrum and have an estimated error of less than 1 nV s. When the pulse moment is higher than 1 A s, the NMR signal starts to increase and reach its peak value at a moment of 2 A s. The extracted envelopes are usable just after the excitation pulse decays to zero and there is no transient distortion at the beginning of the envelopes caused by digital filtering. With SD, the envelopes show similar behaviour, but they are noisier than the results obtained with the SA method and there is a 3 ms distortion at the early-time envelopes shown in Figs 12(c) and (d). Afterwards, the signal parameters s_0, T_2^*, f_L and φ, are estimated from the extracted envelopes above using nonlinear least squares regression proposed by Legchenko & Valla (1998), and the signal model expressed in eq. (1). The 95 per cent confidence interval (CI) of each parameter is also estimated during the regression. The CIs of the estimated parameters from the extracted envelopes using the two methods are shown in Fig. 13.

Comparing the estimated amplitudes and corresponding CIs obtained by SA and SD requires a scaling in order to transform the SA amplitudes into units of Volts. This procedure simply involves division of the SA estimated amplitudes and corresponding CI by the estimated T_2^* value. No scaling is required for the comparison of T_2^*, f_L and φ CIs. Note that the CI values shown in Fig. 13(a) are scaled by the estimated s_0. Comparing the red and blue profiles reveals that the CIs of SA estimated parameters are smaller than those using SD method in nearly all cases. This indicates that SA is expected to produce more reliable and accurate parameters than the SD method.

5.2 High noise scenario

A second groundwater investigation was conducted in an agricultural field at Javngyde, Denmark. The field is approximately rectangular with a length of 600 m and a width of 300 m. It is encircled by roads at the west and south boundary and electric fences in the north and east. There are powerline and communication cables buried along the roads. The centre of the Rx loop is 100 m away from the road and surface NMR data from the site is very noisy. The local Larmor frequency was observed to be 2153 Hz. The NMR excitation pulses were numerically optimized modulated adiabatic sequences sweeping from 100 Hz below resonance ending at the local Larmor frequency (Grombacher 2018). Twenty pulse moments ranging from 0.18 to 3.3 A s were used and 120 stacks were recorded for each moment. The transmitter loop was a 50 × 50 m^2, single turn square coil. The receiver loop was a 9 × 9 m^2, 12-turn coil placed at the centre of the Tx loop. North of the signal loop, a 9 × 9 m^2, 12-turn reference loop was placed at a site 50 m away from the road. The distance between the signal and reference loops was 100 m.

Both the SA and SD methods were used to extract envelopes. With SA, spikes were removed first. Afterwards, reference noise

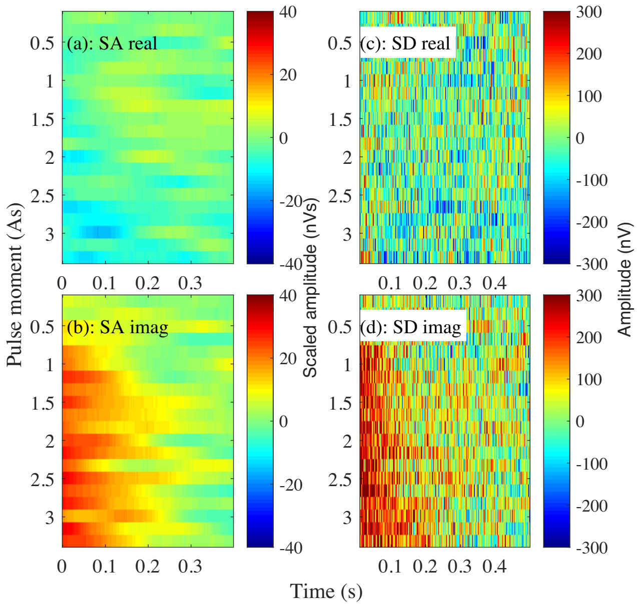

Figure 14. Retrieved (a) real and (b) imaginary envelopes of different pulse moments (*y*-axis) using spectral analysis from the data collected at Javngyde, Denmark. (c) and (d) are the real and imaginary envelopes extracted using synchronous detection from the same data. The colour indicates the scaled amplitude $s_0 T_2^*$ in (a) and (b).

cancellation (RNC) was used to remove correlated noise. Remaining noise from the powerline harmonic component at 2150 Hz was removed by model-based subtraction where the model was fitted to the last 0.5 sec of data and extrapolated to the first part. Subsequently, the data were stacked and envelopes were extracted. The noise spectral density around the Larmor frequency after stacking ranges from 8 to 25 nV Hz$^{-1/2}$. We used an exponential window with a length of 1 s and decay rate of 0.2 s. The selection of the 1 s window produces a 1 Hz passband and helps attenuate the 2150 Hz powerline harmonic. The 0.2 s exponential window is based on the a typical signal relaxation times of 0.2 s and corresponds to a more than 8 times attenuation at the 2150 Hz powerline harmonics. The exponential window helps to reduce the noise energy at the later part of the 1 s window. The sliding step is 100 samples and the window is moved 125 times.

With SD, de-spiking was performed first, followed by filtering with a 1000 Hz bandpass filter centred at 2150 Hz. Next, powerline harmonics, excluding the 2150 Hz component, were removed with the model-based method (Larsen *et al.* 2014). Subsequently, RNC was further used to remove the remaining noise (Müller-Petke *et al.* 2016). The noise in the two loops was highly correlated as they were both close to the buried powerline cables from which the majority of the noise originated.

After RNC, the 2150 Hz powerline harmonic was removed by fitting it to the later part of the signal and extrapolating the model forward to the signal part. Last, the data was stacked and envelopes were extracted. The RMS values of the data before and after RNC are 6 and 1.5 μV, respectively. The RMS value after stacking is about 200 nV. The retrieved envelope profiles are plotted in Fig. 14.

Although the original measurements are very noisy, the spectral analysis method still yields favourable envelopes in Figs 14(a) and (b). As seen in the figure, the amplitude and phase of data from adjacent pulse moments are consistent. When the pulse moment is higher than 1 A s, clear signals can be observed in the real component which matches with the local groundwater table at around 8 m.

In Figs 14(c) and (d), the envelopes using SD method output similar results: only the imaginary parts contain obvious signals. Although filtering, model-based subtraction and reference noise cancellation techniques are applied to remove noise before synchronous detection, the extracted envelopes are still noisy and have lower SNR compared to those retrieved by SA. The noise removal and SD method requires three times the computing time of the SA method and the filter in the SD method increases the dead time by approximately 5 ms.

6 DISCUSSION

The proposed spectral analysis method differs from the commonly used synchronous detection in several ways. Most importantly, the proposed method is only sensitive to the signal and noise exactly at the Larmor frequency and noise at other frequencies can be neglected, within the bounds of leakage inherent to the Fourier transform. The removal of powerline harmonics and random noise with frequencies other than the Larmor frequency are generally not required.

When synchronous detection is employed for envelope extraction, the user has to decide on the characteristics of the lowpass filter used to remove noise after the NMR signal has been frequency shifted to baseband. This choice is a trade-off between transient distortion of the data, which destroys the early and highest amplitude part of the signal, and narrow-band noise filtering, which improves the SNR. Spectral analysis avoids this trade-off by using what can be described as a narrow, non-causal, bandpass filter to directly extract the complex envelope. The frequency response of the spectrum analysis method has much narrower passband than the low-pass filter applied in synchronous detection and the method can therefore yield a higher SNR envelope. Due to the non-causal filtering, the envelope data are immediately available and no additional dead time is added due to transient distortion.

With spectral analysis it is possible to improve the SNR by selecting an optimized window length and shape. In cases where Gaussian noise is superimposed on the NMR signal, the optimum length of a rectangle window is $1.25T_2^*$ and the optimum window is an exponential function e^{-t/T_2^*}. In real measurements, the NMR signal can also be distorted by non-Gaussian noise and the relaxation time is not known in advance. Therefore the choice of optimum window function becomes more complicated. Our experience from processing of field data sets is that if reasonable parameters are initially chosen for window length and shape, the method will yield good results from which NMR parameters can be estimated and used as inputs for a refined reprocessing of the data.

Both spectral analysis and synchronous detection demand knowledge of the Larmor frequency. In spectral analysis, the Fourier transform is performed at Larmor frequency and with synchronous detection the data must be frequency shifted by the Larmor frequency. As such, both methods are sensitive to errors in the Larmor frequency.

We would like to point out that the results presented here are all based on data obtained with our Apsu surface NMR instrument, but the spectral analysis method can also be used with data from commercial manufacturers.

7 CONCLUSION AND OUTLOOK

We have presented a new method for retrieving envelopes and estimating signal parameters of surface NMR data using spectral analysis and a sliding window. Spectral analysis estimates the decaying envelope by Fourier transforming data using sliding windows and tracking the decaying signal at the Larmor frequency. The main benefit of our approach is that only co-frequency noise has significant impact on the results. Moreover, the absence of traditional filtering procedure avoids transient distortion at the early-time signal, which significantly reduces the dead time and improves the reliability of the envelopes. Furthermore, by continuing to work with data in the time-domain, it readily allows one to exploit existing familiarity with the interpretation of time-domain NMR signals.

The Larmor frequency is an important input parameter in the spectral analysis method. We found that if the error in the estimated Larmor frequency is smaller than $\pm$ 0.25 Hz, amplitude errors are below 1 per cent. We demonstrated that the Larmor frequency can be determined by sweeping the estimated frequency and locating the frequency yielding the maximum NMR signal magnitude. Simulation results show that when the scaled amplitude $s_0 T_2^*$ is approximately 10 times higher than the stacked noise spectrum, the estimate error is less than 0.25 Hz. The optimum length of a rectangle window is $1.25T_2^*$. The window that obtains the maximum SNR is exponentially weighted with a decaying rate of T_2^*. In practice, where the relaxation rate is unknown before spectral analysis, a 0.25 s exponential window with $T_\mathrm{w} = 0.5$ s can be applied first and a repeated procedure can be utilized after a preliminary T_2^* is estimated.

Extracted parameters from synthetic signals demonstrate that the spectral analysis method has higher accuracy than the traditional synchronous detection approach. The method not only produces very high quality envelopes from data collected in low noise scenarios, but can also yield useful results from data recorded in high noise environments. The proposed method is numerically efficient and can be easily implemented.

This work has focused on mono-exponential signals, but multi-exponential envelopes can also be extracted with this approach due to the linearity of the Fourier transform. In the next steps of this research we aim to develop a revised kernel function and new inversion algorithm working directly on the scaled amplitude data and evaluate the performance of inversion using scaled amplitude data.

ACKNOWLEDGEMENTS

The work was supported by grants from the Chinese Scholarship Council, the Danish Council for Independent Research, the COWI Foundation and Aarhus University Research Foundation. Two anonymous reviewers are thanked for their comments to improve the manuscript. Gordon Osterman is thanked for assistance with data collection and the final draft of the manuscript.

REFERENCES

Behroozmand, A.A., Auken, E., Fiandaca, G., Christiansen, A.V. & Christensen, N.B., 2012. Efficient full decay inversion of MRS data with a stretched-exponential approximation of the T_2^* distribution, *Geophys. J. Int.,* **190,** 900–912.

Behroozmand, A.A., Keating, K. & Auken, E., 2015. A review of the principles and applications of the NMR technique for near-surface characterization, *Surv. Geophys.,* **36,** 27–85.

Behroozmand, A.A., Auken, E., Fiandaca, G. & Rejkjaer, S., 2016. Increasing the resolution and the signal-to-noise ratio of magnetic resonance sounding data using a central loop configuration, *Geophys. J. Int.,* **205,** 243–256.

Costabel, S. & Müller-Petke, M., 2014. Despiking of magnetic resonance signals in time and wavelet domains, *Near Surf. Geophys.,* **12,** 185–197.

Dabek, J., Nieminen, J.O., Vesanen, P.T., Sepponen, R. & Ilmoniemi, R.J., 2010. Improved determination of FID signal parameters in low-field NMR, *J. Magn. Reson*., **205,** 148–160.

Dalgaard, E., Auken, E. & Larsen, J.J., 2012. Adaptive noise cancelling of multichannel magnetic resonance sounding signals, *Geophys. J. Int.,* **191,** 88–100.

Grombacher, D., 2018. Numerically optimized modulations for adiabatic pulses in surface nuclear magnetic resonance, *Geophysics,* **83,** JM1–JM14.

Grombacher, D., Müller-Petke, M. & Knight, R., 2016. Frequency cycling for compensation of undesired off-resonance effects in surface nuclear magnetic resonance, *Geophysics,* **81,** WB33–WB48.

Grombacher, D., Liu, L., Larsen, J.J. & Auken, E., 2018. Practical considerations for small receive coils in surface NMR, *J. Appl. Geophys.,* **154,** 81–92.

Hertrich, M., 2008. Imaging of groundwater with nuclear magnetic resonance, *Prog. Nucl. Magn. Reson. Spectrosc.,* **53,** 227–248.

Irons, T.P. & Li, Y., 2014. Pulse and Fourier transform surface nuclear magnetic resonance: comprehensive modelling and inversion incorporating complex data and static dephasing dynamics, *Geophys. J. Int.,* **199,** 1372–1394.

Jiang, C., Lin, J., Duan, Q., Sun, S. & Tian, B., 2011. Statistical stacking and adaptive notch filter to remove high-level electromagnetic noise from MRS measurements, *Near Surf. Geophys.,* **6,** 459–468.

Keating, K. & Knight, R., 2006. A laboratory study to determine the effect of iron oxides on proton NMR measurements, *Geophysics,* **72,** E27–E32.

Lachassagne, P., Baltassat, J.M., Legchenko, A. & de Gramont, H.M., 2005. The links between MRS parameters and the hydrogeological parameters, *Near Surf. Geophys.,* **3,** 259–265.

Larsen, J.J. & Behroozmand, A.A., 2016. Processing of surface-nuclear magnetic resonance data from sites with high noise levels, *Geophysics,* **81,** WB75–WB83.

Larsen, J.J.,Dalgaard.E. & Auken, E., 2014. Noise cancelling of MRS signals combining model-based removal of powerline harmonics and multichannel Wiener filtering, *Geophys. J. Int.,* **196,** 828–836.

Legchenko, A. & Valla, P., 1998. Processing of surface proton magnetic resonance signals using non-linear fitting, *J. Appl. Geophys.,* **39,** 77–83.

Legchenko, A. & Valla, P., 2002. A review of the basic principles for proton magnetic resonance sounding measurements, *J. Appl. Geophys.,* **50,** 3–19.

Legchenko, A., Baltassat, J.M., Beauce, A. & Bernard, J., 2002. Nuclear magnetic resonance as a geophysical tool for hydrogeologists, *J. Appl. Geophys.,* **50,** 21–46.

Legchenko, A.V.,Shushakov & O, A., 1998. Inversion of surface NMR data, *Geophysics,* **63,** 75–84.

Liu, L., Grombacher, D., Auken, E. & Larsen, J.J., 2018. Removal of co-frequency powerline harmonics from multichannel surface NMR data, *Geosci. Remote Sens. Lett.,* **15,** 53–57.

Liu, L., Grombacher, D., Auken, E. & Larsen, J.J., 2019. Apsu: a wireless multichannel receiver system for surface-NMR groundwater investigations, *Geosci. Instrum. Method. Data Syst.,* **8,** 1–11.

Lubczynski, M. & Roy, J., 2005. MRS contribution to hydrogeological system parametrization, *Near Surf. Geophys.,* **3,** 131–139.

Müller-Petke, M. & Yaramanci, U., 2010. QT inversion—comprehensive use of the complete surface NMR data set, *Geophysics,* **75,** WA199–WA209.

Müller-Petke, M., Braun, M., Hertrich, M., Costabel, S. & Walbrecker, J., 2016. MRSmatlab—a software tool for processing, modeling, and inversion of magnetic resonance sounding data, *Geophysics,* **81,** WB9–WB21.

Spencer, R.G., 2010. Equivalence of the time-domain matched filter and the spectral-domain matched filter in one-dimensional NMR spectroscopy, *Concepts Magn. Reson. Part A Bridg. Educ. Res.,* **36A,** 255–265.

Smith, J.O., 2011. *Spectral Audio Signal Processing,* 3rd edn, W3K Publishing.

Trushkin, D.V., Shushakov, O.A. & Legchenko, A.V., 1995. Surface NMR applied to an electroconductive medium, *Geophys. Prospect.,* **43,** 623–633.

Vilhelmsen, T.N., Behroozmand, A.A., Christensen, S. & Nielsen, T.H., 2014. Joint inversion of aquifer test, MRS, and TEM data, *Water Resour. Res.,* **50,** 3956–3975.

Walsh, D.O., 2008. Multi-channel surface NMR instrumentation and software for 1D/2D groundwater investigations, *J. Appl. Geophys.,* **66,** 140–150.

APPENDIX: SPECTRUM OF NMR SIGNAL

According to Euler's formula, the real-value measurement in eq. (1) can be written as

$$s(t) = \frac{z(t) + z^*(t)}{2}, \tag{A1}$$

where a$z(t) = s_0 \mathrm{e}^{-t/T_2^*} \mathrm{e}^{i(2\pi f_L t + \varphi)}$nd $z*(t)$ is its complex conjugate. Applying the Fourier transform to $z(t)$,

$$Z(f) = \int_{-\infty}^{\infty} s_0 \mathrm{e}^{-t/T_2^*} \mathrm{e}^{i(2\pi f_L t + \varphi)} \mathrm{e}^{-i2\pi f t} \mathrm{d}t. \tag{A2}$$

Collecting the exponentials give

$$Z(f) = s_0 \mathrm{e}^{i\varphi} \int_0^{\infty} \mathrm{e}^{[-1/T_2^* + i2\pi(f_L - f)]t} \mathrm{d}t. \tag{A3}$$

Note that the integral from $-\infty$ to 0 is removed because there is no signal for $t < 0$.

Thus we get

$$\begin{aligned} Z(f) &= s_0 \mathrm{e}^{i\varphi} \frac{1}{1/T_2^* - i2\pi(f_L - f)} \\ &= s_0 \mathrm{e}^{i\varphi} \frac{1/T_2^* + i2\pi(f_L - f)}{(1/T_2^*)^2 + 4\pi^2(f_L - f)^2}. \end{aligned} \tag{A4}$$

Following the same steps, we can derive $Z*(-f) = Z(f)$, hence

$$\begin{aligned} S(f) &= \frac{Z(f) + Z^*(f)}{2} \\ &= s_0 \mathrm{e}^{i\varphi} \frac{1/T_2^* + i2\pi(f_L - f)}{(1/T_2^*)^2 + 4\pi^2(f_L - f)^2}. \end{aligned} \tag{A5}$$